Knockout Reactions: Analysis, Results and Applications

Arun K. Jain[1*]
[1]*Nuclear Physics Division, Bhabha Atomic Research Centre, Mumbai - 400 085, INDIA*

Recent development of the incorporation of finite range nature of the interaction between the incident particle and the struck particle has led to many startling revelations in the knockout reaction analyses. It removed the huge inconsistencies obtained earlier in the conventional zero-range analyses. In the three body final state reaction of cluster knockout by incident nuclear particle where the residual nucleus not only bears testimony to the dynamics of the knocked out cluster before the event but also testifies the happenings at the time of the hard collision event. In the α -cluster knockout from target nucleus the gross interactions of the two α's with the spectator residual nucleus are large enough to differentiate between the strong peripheral bruising or the deep interpenetration of the two α's. Similar results were witnessed from the heavy cluster knockout in $^{16}O(^{12}C, 2^{12}C)^{4}He$ reaction performed at the Mumbai LINAC. Here the two ^{12}C's were found to have a strong repulsion, where this range is fairly large $\sim 3.7\ fm$. The present results of the large finite range influence in the knockout reactions and their ability to detect change over from repulsive to attractive interaction enhances the possibility of observing the multiquark objects such as Dibaryon and Pentaquark, through nucleon knockout using protons and K^+ mesons. Our approach for the knockout reactions paves the way to include finite range effects in atomic and molecular knockout physics as also in neutron multiplication calculations. The application of FR-DWIA on the heavy cluster knockout reaction opens up new avenues to use the heavy core knockout for the detailed investigation of heavy as well as Borromean halo nuclei.

Knockout reactions are direct reactions where the reaction time is small enough such that there is hardly any time for rearrangement, except for the rearrangement caused by the incident projectile. In knockout reactions simple kinematic energy momentum conservation considerations, along with the assumption that the struck portion of the target behaves as if it were free, lead to the extraction of the momentum distribution of the knocked out cluster from the target before it was knocked out. For almost half a century it was assumed in nuclear reaction physics that the short range nature of the nuclear forces will justify the use of zero range (ZR) approximation for the interaction responsible for knockout. To some extent it was justifiable in (p, 2p), reactions. This ZR-DWIA approximation has the great advantage that the knockout interaction gets separated from the whole matrix element in the form of an off-shell elastic scattering matrix element of the knockout partners. What remains now is the distorted form factor representing the Fourier transform of the bound wave function. The ZR-DWIA being the main reaction model, the same had been applied for the analysis of cluster knockout reactions such as $(p, p\alpha)$, (p, pd), $(\alpha, 2\alpha)$, $(\alpha, \alpha d)$, (α, α^3He), (α, α^3H) etc. on light and medium mass nuclei.

The absolute clustering spectroscopic factors extracted from the cluster knockout reactions with protons as projectiles have been found to be in reasonable agreement with the nuclear structure calculations [1–5]. In the case of cluster knockout reactions using α-particle as projectiles however, there arise orders of magnitude anomalies in the extracted cluster spectroscopic factors [6–11]. So far it had been a puzzle that the ZR-DWIA formalism which seems to work nicely for the $(p, 2p)$, $(p, p\alpha)$, (p, p^3He) and other proton induced knockout reactions fails miserably in predicting very low cross sections

*Electronic address: arunjain@barc.gov.in

for the $(\alpha, 2\alpha)$,$(\alpha, \alpha d)$, (α, α^3He) and other α- induced knockout reactions [10–12]. Exceptions to these observations, however, were seen for the $(\alpha, 2\alpha)$ reactions on ^9Be [13] and ^{12}C at ~ 200 MeV, [14]. The small predictions of absolute cross sections and hence large α - cluster spectroscopic factors from $(\alpha, 2\alpha)$ reactions upto 140 MeV were ascribed to induced α - clustering [6], or in terms of reduced optical distortion effects [15]. These ad hoc prescriptions can not, however, account for the good fits of the ~ 200 MeV data [13, 14].

1. Entrance Channel Potential

There existed some uncertainties about the entrance channel distorting potentials for knockout reactions. The entrance channel potential for the knockout reaction is strictly the potential for the scattering of the incident particle from the residual nucleus which is to be averaged over the volume of the target nucleus [1]. Such a potential is not obtainable from any realistic experiment, therefore most of the DWIA calculations use potentials which reproduce the scattering data on the target nucleus, A but with a scaling down factor [1] equal to the ratio of the mass numbers of the residual nucleus and the target nucleus, $\frac{B}{A}V_{aA}$. This procedure had been adopted in almost all the knockout DWIA calculations.

Recently a single folding procedure for the entrance channel optical potentials has been workedout [16]. For the $A(a, ab)B$ knockout reaction, the single folding model (SFM) effective interaction of the incident particle, a with the target nucleus, A is evaluated in terms of its interactions with the residual nucleus, B and the struck particle, b. These interactions are folded over the density distribution of the target, which can be approximated by the square of the ground state inter-cluster radial wave function.

$$V_{aA} = \int [t_{ab}(\vec{r}_{ab} - \frac{B}{A}\vec{R}) + t_{aA}(\vec{r}_{aA} + \frac{b}{A}\vec{R})]\rho(r)d\vec{R}$$

As the projectile-ejectile, a-b interaction is completely accounted to all order's by the corresponding knockout t-matrix, is to be neglected while evaluating the entrance channel

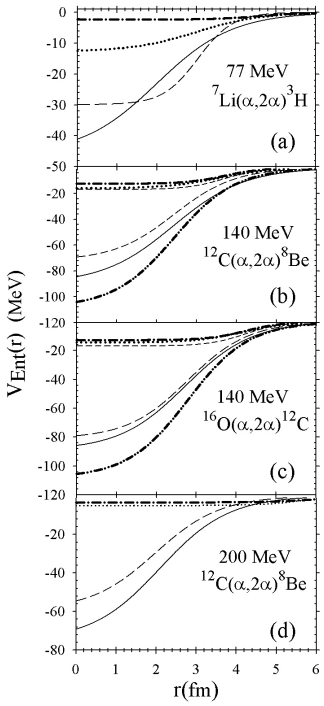

FIG. 1: Various entrance channel optical potential, (——) Real folded, $(\cdots\cdots)$ Imaginary Folded, $(- - -)$ Real $\frac{B}{A}V_{aA}$ prescription and $(- \cdot - \cdot - \cdot)$ Imaginary $\frac{B}{A}V_{aA}$ Prescription. The 140 MeV results used $(- \cdots - \cdots -)$ Real V_{aA} and (_ _ _) Imaginary V_{aA} optical potentials. Fig (a) is for 77 MeV $^7Li(\alpha, 2\alpha)^3H$, (b) is for 140 MeV $^{12}C(\alpha, 2\alpha)^8Be$, (c) is for 140 MeV $^{16}O(\alpha, 2\alpha)^{12}C$ and (d) is for 200 MeV $^{12}C(\alpha, 2\alpha)^8Be$ reactions [16].

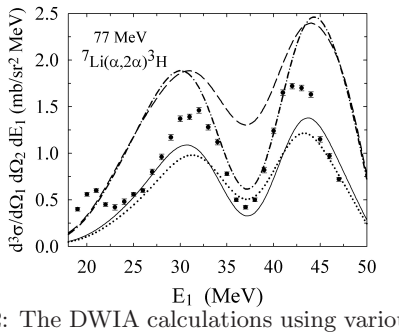

FIG. 2: The DWIA calculations using various entrance channel potentials, $(- - -)$ Warner *et el*, $(- \cdot - \cdot - \cdot)$ 0.7 times Warner *et el*, $(\cdot\cdot\cdot\cdot\cdot)$ folded V_{aA} and (——) 0.8 times folded V_{aA} compared with 77 MeV $^7Li(\alpha, 2\alpha)^3H$ [16].

distorting potentials $V_{Ent}(r)$ for the knockout reaction. On the other hand the effective interaction between a and B, $t_{aB}(\vec{r}_{aB})$ may be approximated by the a-B optical potential, $V_{aB}(\vec{r}_{aB})$. Therefore.

$$V_{Ent}(\vec{r}_{aA}) = \int V_{aB}(\vec{r}_{aA} + \frac{b}{A}\vec{R})\rho(R)d\vec{R}$$

Using this procedure, the entrance channel optical potentials have been evaluated [16] for various reactions such as $^7Li(\alpha, 2\alpha)^3H$, $^{12}C(\alpha, 2\alpha)^8Be$, $^{16}O(\alpha, 2\alpha)^{12}C$ and many other α cluster knockout reactions at various energies (See Fig.1). In this figure all the folded entrance channel potentials are seen to be much different from the ones obtained from either the $\frac{B}{A}$ prescription or the V_{aA} approximation. Both the real and imaginary folded potentials are seen to be deeper than the corresponding $\frac{B}{A}V_{aA}$ potentials. The potentials employed for the analyses of the 140 MeV data by Wang *et al* [6], however, are deeper than the folded potentials.

For the 77 MeV $^7Li(\alpha, 2\alpha)^3H$ reaction results for folding and $\frac{B}{A}$ prescription are compared with the data in (Fig.2). It is seen in this figure that while the shapes agree reasonably well with each other the folding model results are smaller by almost a factor two in absolute magnitude. In both the calculations the dip at the zero recoil momentum position is seen to be still filled up in comparison to the experimental results. It is also seen that when the entrance channel potential depths, both in the $\frac{B}{A}$ as well as in the folding criterion, are reduced by about 25 % the peak to valley ratio increases sharply in better agreement with the data. In the ℓ=0 knockout also the shape of the single peaked spectra do not change much but using the folding criterion the cross section is reduced by half in comparison to the $\frac{B}{A}$ criterion.

For the entrance channel optical potentials it can therefore can be concluded that in the conventional DWIA prediction of the ℓ=1 knockout spectra the discrepancy in the peak to dip cross section ratio arises mainly due to the uncertainties in the choice of the entrance channel potentials. The use of folded potentials are seen to change the DWIA predictions for absolute cross sections. Above all, the use of the cluster folding potentials appear to be more consistent and aesthetically more satisfying.

2. Finite Range t-Matrix

One of the basic approximations which has been explicitly used in the conventional DWIA analyses of the knockout reactions is the factorization approximation (FA). Empirical tests of this factorization approximation have been obtained in $(\alpha, 2\alpha)$ reactions in various kinematic conditions. Theoretically, however, it has been argued [17, 18] that the factorization may arise not only due to the short range nature of the t-matrix effective interaction but may also arise due to the constancy of the optical distortion factors over the significant range of the t-matrix effective interaction. For example in the extreme case of no optical distortions or in other words the plane waves the factorization would be exact even when the t-matrix effective interaction is of sufficiently large range. As the ratio of the PWIA to the DWIA cross sections, $(\frac{\sigma_{PW}}{\sigma_{DW}})|_{(\alpha,2\alpha)}$ in table(II) of ref [1], is more than 3-orders of magnitude, which implies that the distortion effects are too large. The saving grace however is that the experimental results are very close to the PWIA, indicating thereby that the distortion effects are very much over estimated in the ZR-DWIA through the factorization approximation.

The important finding in the comparison of FR-DWIA and ZR-DWIA for $(p, 2p)$ reactions [19–21] is to witness large differences in shapes and magnitudes of their energy sharing distributions. While the p-p t-matrix effective interaction was available [22, 23] for doing the FR-DWIA calculations for $(p, 2p)$ reactions the α-α t-matrix effective interaction was not available for the FR-DWIA analysis of $(\alpha, 2\alpha)$ reactions in the literature. We therefore evaluated the $\alpha - \alpha$ t-matrix effective in-

teraction [24] using the basic definition,

$$T^{\pm} = V\Psi^{\pm} \tag{1}$$

where T, V,Φ, and Ψ are the t-matrix effective interaction, the realistic interaction, the plane wave scattering state and the realistic scattering state wave function with proper asymptotic boundary condition. For $(\alpha, 2\alpha)$ reaction the $t_{\alpha\alpha}$-matrix is now to be evaluated using the α-α potential V which fits the α-α elastic scattering data. The α-α t-matrix effective interaction, $t^{+}_{\alpha\alpha}(E,\vec{r})$ takes the form as,

$$t^{+}_{\alpha\alpha}(E,\vec{r}) = e^{-\imath kz}C(\vec{r})\Psi^{+}_{\alpha\alpha}(\vec{r})$$

$$\equiv \sum_{L=0,1,2,3...} t_L(E,r)P_L(\hat{r}) \tag{2}$$

Here it is to be noted that all the multipole L-values (=0,1,2,3..), even as well as odd, contribute in the expansion of the above equation. Then,

$$t_L(E,r) = (L+\frac{1}{2})\sum_{\ell,m} V_\ell(r)i^{\ell+3m}(2\ell+1)(2m+1)$$
$$e^{\imath\sigma_\ell}\int_{-1}^{+1} P^*_L(t)P_\ell(t)P_m(t)dt\jmath_m(kr)\frac{u_\ell(kr)}{kr} \tag{3}$$

Where $\jmath_m(kr)$ is the spherical Bessel function and $u_\ell(kr)$ is the radial wave function obtained from the solution of the Schrodinger equation for α-α scattering.

Using the α-α elastic scattering data one can obtain the optical potentials which are mostly L-independent and have at the most 6 to 9 free parameters which are constrained with in permissible limits due to specific reasoning and logic. It so turned out that there are many sets of optical potentials which fit the elastic scattering. These sets have continuous as well as discrete ambiguities. Besides this uncertainty there are two distinct types of optical potentials used for α-α scattering, and some other scattering systems, one of these types are the all-through attractive potentials and the other types are the L-dependent potential having a repulsive core [25]

It had been seen that a choice of the real part of the α-α optical potential as a sum of two attractive Woods-Saxon forms provide excellent fits to the α-α scattering data over a wide range of energies. Thus these two types of optical potentials, widely differing in their shape, their energy and angular momentum dependence, reproduce the elastic scattering data equally well. It is thus to be emphasized that so far there has been no way to choose one type of optical potential to the other type in their suitability for other applications. The t-matrix effective interactions, $t_L(r)$ for repulsive core and all-through attractive α-α interactions as seen in figs. 3(a) and 3(b)respectively are drastically different from their respective realistic interactions. Moreover, the basic character of the $t_{\alpha\alpha}(r)$'s, from the repulsive core α-α optical potential and from the all-through attractive α-α optical potential is drastically different. Most notable is the vanishing of the effective interaction from the region of the repulsive core region of the optical potential.

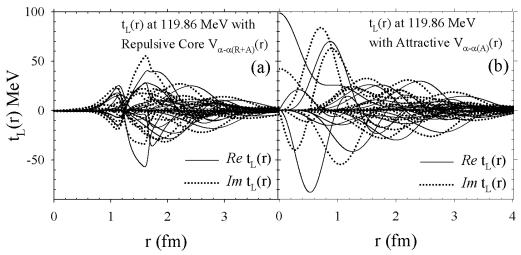

FIG. 3: Effective α-α t-matrix interaction, $t_L(r)$ vs r at 119.86 MeV for many L-values, (a) using $V_{\ell,\alpha\text{-}\alpha}(r)$ with repulsive core and a longer range attraction, (b) using a purely attractive $V_{\alpha\text{-}\alpha}(r)$. [26]

3. FR-DWIA Calculations

Having obtained the t-matrix for the $\alpha-\alpha$ scattering using the optical potentials we are now ready to formulate the transition amplitude, T_{fi} for the knockout reaction A$(\alpha, 2\alpha)$B in the FR-DWIA formalism from the initial state, i to the final state, f. It can be written [2, 17, 18],

$$\frac{d^3\sigma^{L,J}}{d\Omega_1 d\Omega_2 dE_1} = F_{kin}\cdot S^{LJ}_{\alpha}\cdot\sum_{\wedge}|T^{\alpha L\wedge}_{fi}(\vec{k}_f,\vec{k}_i)|^2 \tag{4}$$

where J and L ($\wedge$) are the total and orbital

(its azimuthal component) angular momenta of the bound α-particle in the target nucleus, F_{kin} is a kinematic factor and S_α^{LJ} is the cluster spectroscopic factor. The conventional transition matrix element for the knockout reaction, $T_{fi}^{\alpha L\wedge}(\vec{k}_f, \vec{k}_i)$ using the finite range α-α t-matrix effective interaction $t_{12}(\vec{r}_{12})$ is given by [2, 17, 18]:

$$T_{fi}^{\alpha L\wedge}(\vec{k}_f, \vec{k}_i) = \int \chi_1^{(-)*}(\vec{k}_{1B}, \vec{r}_{1B})\chi_2^{(-)*}(\vec{k}_{2B}, \vec{R}_{2B}) t_{12}(\vec{r}_{12})\chi_0^{(+)}(\vec{k}_{1A}, \vec{r}_{1A})\varphi_{L\wedge}(\vec{R}_{2B})d\vec{r}_{12}d\vec{R}_{2B} \quad (5)$$

The distorted waves χ_0, χ_1 and χ_2 of Eq.5 are evaluated using the optical potentials for the α_1-A, α_1-B and α_2-B. Finally all the relative coordinates are expressed in terms of $\vec{r}_{12}(\equiv \vec{r})$ and $\vec{R}_{2B}(\equiv \vec{R})$. While using the ZR-DWIA the transition matrix element, T_{fi} of Eq. 5 was factorized into integrals over $\vec{r}$ and $\vec{R}$ separately. The same is not possible when one uses the full finite range $t_{12}(\vec{r}_{12})$ due to the presence of optical distortions. This is because in the FR-DWIA formalism the chosen relative coordinates $\vec{r}$ and $\vec{R}$ get coupled through the distorted waves $\chi_0^{(+)}(\vec{k}_{1A}, \vec{r}_{1A})$ and $\chi_1^{(-)*}(\vec{k}_{1B}, \vec{r}_{1B})$.

For the evaluation of $T_{fi}^{\alpha,L,\wedge}$ of Eq.5 the distorted waves, $\chi(\vec{k}, \vec{r})$ were expanded in terms of partial waves and then on the mesh of the spherical polar coordinates, r, θ, ϕ and R, Θ, Φ the values of χ_0, χ_1, χ_2, $\varphi_{L\wedge}(\vec{R})$ and $t_{12}(\vec{r})$ were evaluated. The final result of T_{fi} is obtained by doing a 6-dimensional integration over the mesh of $\vec{r}$ and $\vec{R}$ coordinates. The computer code was checked by performing FR-plane wave impulse approximation (PWIA) calculations using the present 6-dimensional integration approach as well as through the 3-dimensional integrations approach (because in the plane wave case the 6-dimensional integral of Eq. 5 factorizes into two 3-dimensional integrals, one over $\vec{r}$ and the other over $\vec{R}$).

We performed the FR-DWIA analyses of the typical (α,2α) data on ^{9}Be at 197 [13] and 140 MeV [6], on ^{12}C at 200 [14] and 140 MeV [6] and on ^{16}O at 140 [6] and 90 MeV [**?**]. For these analyses, out of the many possible $t_{12}(\vec{r})$'s, we used the α-α t-matrix effective interactions obtained from the two types of α-α optical potentials, attractive with a repulsive core, (R+A) on the one hand and all-through attractive, (A) on the other hand.

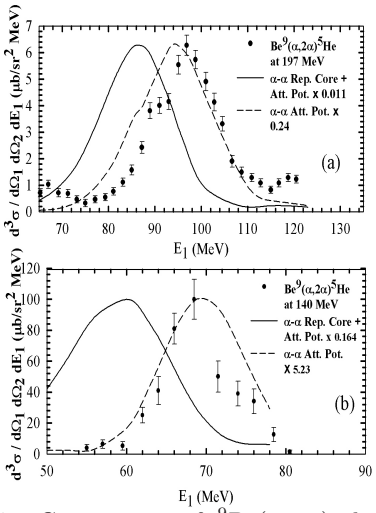

FIG. 4: Comparison of ^{9}Be($\alpha, 2\alpha$) data with the FR-DWIA calculations using α-α interaction which is purely attractive(A) and having a repulsive core (R+A), (a) for 197 MeV and (b) for 140 MeV [26].

In the calculations we employed the improved prescription for the entrance channel potentials [16] where the folding model replaces the conventional ($\frac{B}{A}$) prescription [1]. The α_2-B bound wave function, $\varphi_{L\wedge}(\vec{R})$ is generated as usual for the Woods-Saxon form with R_{bound}=1.09 $B^{\frac{1}{3}}$ fm.

The results of the FR-DWIA computations, normalized to the data peak values, are presented in Figs.4, 5 and 6. The curves obtained from the attractive, $t_{\alpha\alpha(A)}(\vec{r})$ are much closer to the data. This arises because the $t_{\alpha\alpha(A)}(\vec{r})$'s peak close to r=0, which simulates the zero range behavior and hence the results are similar to the ZR-DWIA results [1]. The repulsive core, (R+A) results are seen to be at much variance. This could arise due to the uncertainty in the choice of the repulsive core α-α potential parameters. Most important con-

TABLE I: Comparison of (α, 2 α) cross sections from FR-DWIA calculations and experimental data on ^{9}Be, ^{12}C and ^{16}O at various energies and spectroscopic factors (S_α) derived from the FR-DWIA calculations and theory. Comparison of Bold face entries is emphasized [26].

Reaction	E_α	$\sigma_{\alpha,2\alpha}(Peak)/\mathrm{Sr}^2\mathrm{MeV}$				S_α			
	(MeV)	(R+A)	(A)	Expt	Ref.	(R+A)	(A)	Theory	Ref.
$^{9}\mathrm{Be}(\alpha,2\alpha)^{5}\mathrm{He}$	197	575 μb	**26.4** μb	**6.3** μb	[13]	0.011	**0.24**	**0.57**	[4]
	140	**609** μb	19.1 μb	**100** μb	[6]	**0.164**	5.23		
$^{12}\mathrm{C}(\alpha,2\alpha)^{8}\mathrm{Be}$	200	19.9 μb	**552** nb	**380** nb	[14]	0.02	**0.7**	**0.55**, **0.29**	[4, 5]
	140	**92** μb	2.5 μb	**18.5** μb	[6]	**0.2**	7.4		
$^{16}\mathrm{O}(\alpha,2\alpha)^{12}\mathrm{C}$	140	**19.1** μb	0.51 μb	**10.5** μb	[6]	**0.55**	20.6	**0.23**, **0.3**	[4, 5]
	90	**171** μb	14.3 μb	**68** μb	[**?**]	**0.4**	4.75		

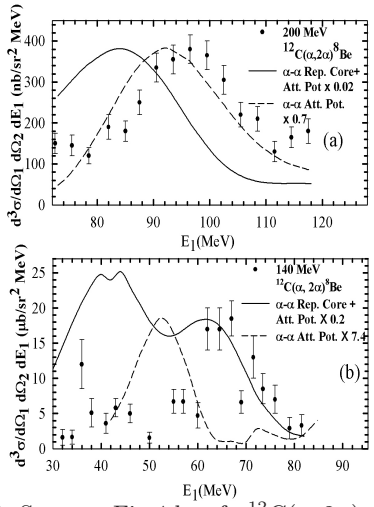

FIG. 5: Same as Fig.4 but for$^{12}\mathrm{C}(\alpha,2\alpha)$ reaction, (a) for 200 MeV and (b) for 140 MeV [26].

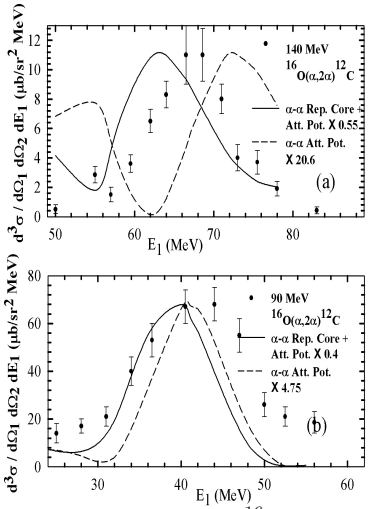

FIG. 6: Same as Fig.4 but for $^{16}\mathrm{O}(\alpha,2\alpha)$ reaction, (a) for 140 MeV and (b) for 90 MeV [26].

clusion however, can be drawn by comparison (bold face entries) of the absolute peak cross section values from the FR-DWIA calculations with the data and the derived S_α-values with the structure theory estimates [4, 5] in Table. I.

In Table. I it is seen that the absolute cross sections and S_α values for the $\sim$ 197-200 MeV $(\alpha, 2\alpha)$ reactions on ^{9}Be and ^{12}C using the purely attractive $t_{\alpha\alpha(A)}(\vec{r})$ are in better agreement with data in comparison to that using $t_{\alpha\alpha(R+A)}(\vec{r})$ where the absolute cross sections are 20 to 35 times larger. For energies at and below $\sim$ 140 MeV, both the $t_{\alpha\alpha(A)}(\vec{r})$ and $t_{\alpha\alpha(R+A)}(\vec{r})$ yield somewhat distorted shapes. Yet the peaks close to the zero recoil momentum position (normalized to the data peak values) yield S_α-values, seen in Table.1, much closer to the theoretical values when $t_{\alpha\alpha(R+A)}(\vec{r})$'s are employed. On the other hand, the S_α-values obtained from the $t_{\alpha\alpha(A)}(\vec{r})$'s are 10 to 90 times too large as compared to the theoretical estimates [4, 5].

Differences of almost two orders of magnitude are seen between the FR-DWIA predictions of the (α, 2α) reaction cross sections using the repulsive core, (R+A) and purely attractive, (A) α-α potentials. An obvious conclusion is that use of the conventional ZR-DWIA formalism and hence the factorization approximation for the analysis of (α, 2α) reactions below $\sim$197 MeV was incorrect.

While, due to factorization, the FR-PWIA (α, 2 α) results for the (R+A) and (A) α-α

potentials match, the enhancement of the FR-DWIA results for the (R+A) case over that of the (A) case can be understood qualitatively. It is to be visualized that due to the α-α repulsion the incident α-particle can knockout the bound α-cluster while remaining outside the absorbing region. On the other hand when the α-α interaction is purely attractive the $t_{\alpha\alpha(A)}(\vec{r})$ peaks at r=0 and hence the α_1 has to enter the absorbing region to knock the bound α_2 out. Thus the enhancement in the (R+A) case arises due to the reduction in the optical absorption as a result of the α-α repulsion.

From these FR-DWIA results it is obvious that the α-α potential character changes drastically at α-energies, E_α somewhere between 140 and 200 MeV, corresponding to $E_{\alpha\text{-}\alpha}$ of 70 to 100 MeV. It can be qualitatively understood in the Resonating Group Method, (RGM)-shell model picture (taking care of Pauli's exclusion principle). Here the four neutrons(n) and four protons(p) of the two α-particles can exist in an overlapping position if the two n's and two p's of one α-particle are in the lowest $1s_{1/2}$ shell model state and the other two n's and two p's of the other α in the next shell model state ($1p_{3/2}$, which is situated around 21 MeV above the ground state of α-particle). The total energy of this overlapping system, $E_{\alpha\text{-}\alpha}$ will thus be $\sim$4×21=84 MeV (corresponding to E_α $\sim$2×84=168 MeV). Thus below E_α $\sim$168 MeV, the two α's would find it energetically more favorable to avoid their overlap with a repulsive core in their interaction. Above this energy, however the two α's have no such restriction and are free to have the usual attractive force between them. This understanding of the change in the nature of the α-α interaction is clearly validated by the present FR-DWIA analyses of the (α, 2α) data.

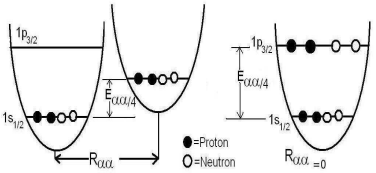

FIG. 7: Shell model (RGM) scheme of two α-particles when separated or overlapping at relative energy of $E_{\alpha\text{-}\alpha}$ [26].

Similar arguments with repulsive core, (R+A) interaction between α-d, α-t and α-^{3}He are expected to remove the inconsistencies [10] in the (α, αd), (α, αt) and (α, α ^{3}He) reactions in comparison to the corresponding knockout reactions using the proton projectiles.

4. Heavy Cluster Knockout

As the large anomalies of the (α, 2α) reactions may be understood in terms of the finite size of the α-α knockout vertex. Based on this finding, a heavy cluster knockout reaction, $^{16}O(^{12}C, 2^{12}C)^4He$ has been conceptualized and executed for the first time so as to reveal the true short distance behaviour of the ^{12}C-^{12}C knockout vertex.

This reaction is expected to differentiate between the highly attractive (as obtained in the double folding model, (DFM) [27, 28] and L-dependent repulsive core (as obtained in the resonating group method, (RGM)) ^{12}C-^{12}C interaction [29, 30]. It was found impossible to discriminate between these two kinds of ^{12}C-^{12}C interactions from the analysis of the ^{12}C-^{12}C elastic scattering data alone, see Fig. 8.

The beauty of the $^{16}O(^{12}C, 2^{12}C)^4He$ reaction, as seen in Fig. 9, is that it differs from the $^{16}O(\alpha, 2\alpha)^{12}C$ [1, 6] reaction essentially in the knockout vertex (^{12}C-^{12}C vs α-α). The inter-cluster bound wave function due to the α-^{12}C bound state component of ^{16}O) [1, 2, 14] as well as the optical distortions (α-^{12}C optical potentials (except for some energy dependence [31, 32] are the same. Due to the larger size of the ^{12}C-nucleus compared to that of the α-particle ($\sim$1.5 times) the finite range effects in the (^{12}C,^{12}C) reaction cross

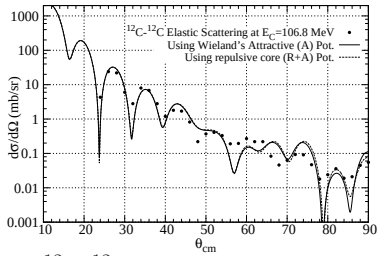

FIG. 8: ^{12}C-^{12}C elastic scattering using all-through attractive (A) optical potential Weiland *et al* and L-dependent (R+A) optical potential.

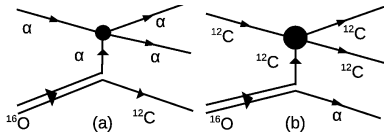

FIG. 9: First order knockout diagram for a) $^{16}O(\alpha, 2\alpha)^{12}C$, b) $^{16}O(^{12}C, 2^{12}C)^4He$ reaction.

sections are expected to be more enhanced than that in the (α, 2α) reaction [1, 6, 15].

The experiment was performed at Pelletron-LINAC facility at Mumbai using $\sim$2.5 pnA 118.8 MeV ^{12}C beam. A target with WO_3 of Oxygen content equivalent of $\sim$ 36.2 $\mu g/cm^2$ was used. The knockout of ^{12}C from W can be easily separated because of its large positive Q-value.

The summed energy spectrum is seen in Fig. 10 where one can easily identify the two prominent broad peaks marked by arrows separated by $\sim$ 4 MeV. The higher (E_1+E_2) peak corresponds to the two correlated ^{12}C's emitted in their ground state, and the second peak corresponds to the decayed 4.44 MeV excited state of one ^{12}C in coincidence with the other ^{12}C in its ground state. The energy sharing spectrum ($\frac{d^3\sigma}{d\Omega_1 d\Omega_2 dE_1}$ vs E_1) is shown in Fig. 11. The broad peak in this spectrum (akin to the ℓ=0 knockout) occurred at E_1 $\simeq$57 MeV with recoil momentum, p_3 $\simeq$41 MeV/c. The uncertainty in the absolute cross section is estimated to be around 30 %

A conventional ZR-DWIA estimate of the present reaction was performed. Compared to the experimental peak cross section value of $\sim$ 125 $\pm$ 50 $\mu b/$ Sr^2MeV the two aforementioned ZR-DWIA prescriptions (B/A and SFM) provide the values of 3.23 and 0.56 μb / Sr^2 MeV respectively (Spectroscopic factors 36.7 and 222 respectively). The plane wave impulse approximation (PWIA) provided this value to be 290 μb /Sr^2 MeV, with a spectroscopic factor, S_F $\sim$ 0.43 much closer to the value of 0.23 , from structure theoretical estimates [4, 5].

For the present case of $^{16}O(^{12}C, 2^{12}C)^4He$ reaction only the attractive optical potentials (see Fig. 12(1)) was available to fit the ^{12}C-^{12}C elastic scattering. Using a repulsive core radius of 3.65 fm a ^{12}C-^{12}C L-dependent optical potential of short range repulsion and

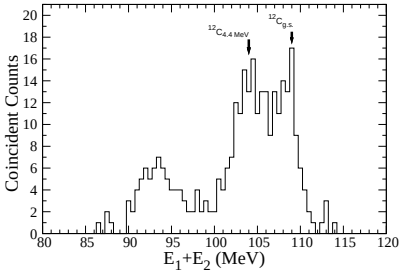

FIG. 10: Summed energy spectrum for the 118.8 MeV $^{16}O(^{12}C, 2^{12}C)^4He$ reaction, the peaks corresponding to both $^{12}C's$ in their ground states and one ^{12}C in ground state and another in first excited state (4.44 MeV) are identified.

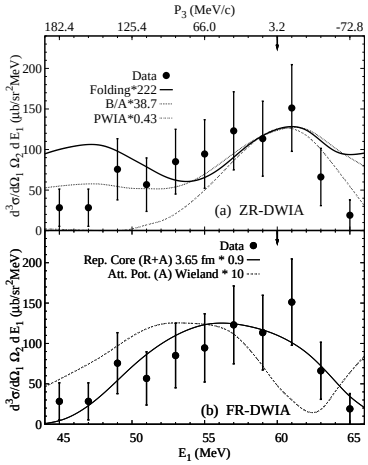

FIG. 11: Energy sharing spectrum for the 118.8 MeV $^{16}O(^{12}C, 2^{12}C_{g.s})^4He$, compared with calculations (normalized to the peak) (a)($\cdots\cdots$) PWIA, and ZR-DWIA results using entrance channel optical potential, ($\cdots$) B/A prescription and (—-) SFM prescription, (b) FR-DWIA results (——) using 3.65 fm repulsive core, (R+A) ^{12}C-^{12}C potential and ($\cdots$) all through attractive, (A) ^{12}C-^{12}C optical potential of Weiland et al. [27]

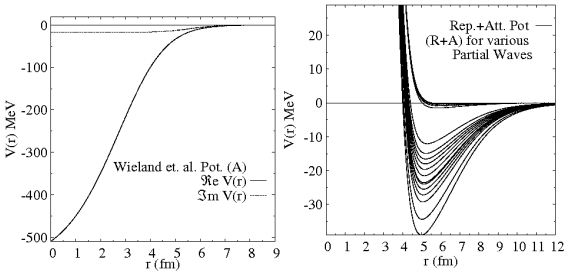

FIG. 12: ^{12}C-^{12}C optical potential $V_{C-C}(r)$ 1) all through attractive (A), 2) with L-dependent repulsive core (R+A).

longer range attraction (R+A) was obtained by fitting the various phase shifts from the all-through attractive, (A) optical potential.

The FR-DWIA calculations for the energy sharing distributions, $\frac{d^3\sigma}{d\Omega_1 d\Omega_2 dE_1}$ vs E_1 of the $^{16}O(^{12}C, 2^{12}C)^4He$ reaction are compared in Fig. 12(b). The calculations (normalized to the peak) are seen to be nicely reproducing the shape of the experimental distribution for the repulsive core, (R+A) ^{12}C-^{12}C t-matrix while use of the attractive, (A) t-matrix shifts the distribution. The absolute cross sections for the all-through attractive,(A) t-matrix and with the repulsive core, (R+A) are 12.5 μb/Sr^2 MeV and 136.7 μb/S$r^2 MeV$ respectively. The corresponding spectroscopic factors of 10 and 0.9 respectively are to be compared with structure theoretical estimate of 0.23. The reasonable (R+A)-fit (within the uncertainties of the experimental absolute cross section as well as those associated with the theoretical estimates) leads us to the conclusion that the ^{12}C-^{12}C interaction around 105 MeV should have a repulsive core. This finding is quite contrary to the conclusion arrived at by the proponents of the double folding model prescription for ^{12}C-^{12}C interaction around 100-140 MeV incident energy.

Our finding of repulsion in the ^{12}C-^{12}C interaction (below $r \sim 3.65\ fm$) to explain the $^{16}O(^{12}C, 2^{12}C)^4He$ reaction data is in conflict with the findings of large attraction at these distances from the double folding model. Criticism of the double folding model arises from the use of unjustified nucleon-nucleon (N-N) M3Y- effective interaction as also from the failure in accounting for the proper antisymmetrization of ^{12}C-^{12}C microscopic wave function in the double folding model. The M3Y-effective interaction peaks at r=0 while it has been clearly shown by us [24] that any effective interaction between particles having a short range repulsion, as is the case with nucleons, the effective interaction has to vanish in the region of strong repulsion. Even the use of density dependent (N-N) effective interaction [33] has the drawback that it does not predict the transition from repulsive core to strong attraction at some definite energy as seen in the (α, 2α) case.

5. Conclusions

It is a clear message from our present work that heavy ion optical potentials in this energy region have highly repulsive core and the attractive potentials obtained from the double folding model are incorrect and unsuitable for describing the absolute cross sections of the knockout reactions. Subsequently it reflects on the reliability as well as the density and energy dependence of the effective N-N interaction. The heavy cluster knockout reaction of the $^{16}O(^{12}C, 2^{12}C)^4He$ type can therefore prove to be a nice tool for determining the true nature of the short range component of the heavy ion interaction as also the applicability of the RGM formalism to find the proper heavy ion potentials.

The $^{16}O(^{12}C, 2^{12}C)^4He$ reaction, performed at 118.8 MeV. It is first of its kind where exclusive measurements of the heavy cluster knockout are performed and will thus be even more informative in the case of heavy cluster knockout from heavy nuclei as also from the Halo nuclei, for example ^9Li knockout from the ^{11}Li beam in the $^9Be(^{11}Li,^9 Li^9Be)2n$ reaction and α knockout from ^6He in the $^4He(^6He, 2\alpha)2n$ reaction.

Other heavy cluster knockout reaction such as $^{24}Mg(^{12}C, 2^{12}C)^{12}C$, $^{32}S(^{16}O, 2^{16}O)^{16}O$ etc can be used to study di-nuclear molecular structure of heavier nuclei as also for studying the halo nuclei such as ^{11}Li, ^6He etc. Heavy cluster knockout may also be invoked to check the application of the effective N-N interaction in the reaction dynamics.

Extreme sensitivity of the cluster knockout reactions to the short range behavior of the colliding partners opens up the possibility of probing this aspect of the particles involved at the knockout vertex. In $(p, 2p)$ reactions for example, one should be able to see the behavior of the nucleon-nucleon interaction at short distances or otherwise, if there is a possibility of dibaryon formation at some energy then one should be able to decipher it from the FR-DWIA analyses of the $(p, 2p)$ reactions

[20]. Similarly one can visualize observing the Δ-resonance in $(\pi, \pi p)$ reaction [34] and the pentaquark, Θ^+ [35] in (K^+, K^+n) reaction due to enhanced distortion effects. In heavy ion knockout reactions also one can investigate the short range behavior of the heavy ions involved at the knockout vertex which is rather difficult to observe in the elastic scattering. The present results and conclusions may be very instructive in studies involving $(e, 2e)$ reactions on atoms, knockout of atoms from molecules, $(n, 2n)$ reactions for neutron multiplication and in many other disciplines involving direct knockout reactions.

References

[1] N. S. Chant and P. G. Roos, Phys. Rev. C **15**, 57 (1977).
[2] P. G. Roos *et al.*, Phys. Rev. C **15**, 69 (1977).
[3] T. A. Carrey *et al.*, Phys. Rev. C **23**, 576 (1981).
[4] D. Kurath, Phys. Rev. C **7**, 1390 (1973).
[5] M. Ichimura *et al.*, Nucl. Phys. ***A*204**, 225 (1973).
[6] C. W. Wang *et al.*, Phys. Rev. C **21**, 1705 (1980).
[7] N. S. Chant and P. G. Roos, C. W. Wang, Phys. Rev. C **17**, 8 (1978).
[8] R. E. Warner *et al.*, Phys. Rev. C **45**, 2328 (1992).
[9] A. K. Jain and S. Mythili, Phys. Rev. C **53**, 508 (1996).
[10] C. Samanta *et al.*, Phys. Rev. C **26**, 1379 (1982).
[11] C. Samanta *et al.*, Phys. Rev. C **35**, 333 (1987).
[12] Arun K. Jain, Phys. Rev. C **45**, 2387 (1992).
[13] A. A. Cowley *et al.*, Phys. Rev. C **50**, 2449 (1994).
[14] G. F. Steyn *et al.*, Phys. Rev. C **59**, 2097 (1999).
[15] A. K. Jain and N. Sarma, Nucl. Phys. A **321**, 429 (1979).
[16] Arun K. Jain and B. N. Joshi, Phys. Rev. C **77**, 027601 (2008).
[17] D. F. Jackson and T. Berggren, Nucl. Phys. **62**, 353 (1965).
[18] G. Jacob and Th. A. J. Maris, Rev. Mod. Phys. **38**, 121 (1966).
[19] Y. Kudo *et al.*,Xth Int. Conf on Particles and Nuclei, (PANIC''87,Kyoto 1987)p 374.
[20] E. D. Cooper and O. V. Maxwell, Nucl. Phys. ***A*493**, 468 (1989).
[21] Y. Ikebata, Phys. Rev. C **52**, 890 (1995).
[22] W. G. Love and M. A. Franey, Phys. Rev. C **24**, 1073 (1981).
[23] M. A. Franey and W. G. Love, Phys. Rev. C **31**, 488 (1985).
[24] Arun K. Jain and B. N. Joshi, Prog. of Theor. Phys **120**, 1193 (2008).
[25] P. Darriulat *et al.*, Phys. Rev. C **137**, B315 (1965).
[26] Arun K. Jain and B. N. Joshi, Phys. Rev. Lett. **13**, 132503 (2009).
[27] R. M. Weiland *et al.*, Phys. Rev. Lett. **37**, 1458 (1976).
[28] G. Delic, Phys. Rev. C **41** 2032 (1990).
[29] H. Friedrich and L. F. Canto, Nucl. Phys. A **291** 248 (1977).
[30] K. Aoki and H. Horiuchi, Prog. Theor. Phys. **66** 1508 (1981).
[31] S. Hossain *et al.*, Phys. lett. ***B*626**, 248 (2006).
[32] E. B. Carter *et al.*, Phys. Rev. **133**, B1421 (1964).
[33] B. Sinha, Phys. Rep. **20**, 1(1975).
[34] S. H. Yoo, *et al.*, Phys. Rev. Lett. **63**, 738 (1989).
[35] T. Nakano, *et al.*, Phys. Rev. C **79** 025210 (2009).